2016 IEEE-RAS 16th International Conference on
Humanoid Robots (Humanoids)
Cancun, Mexico, Nov 15-17, 2016

# Planning robust walking motion on uneven terrain via convex optimization

Hongkai Dai[1,2] and Russ Tedrake[1,2]

***Abstract*— In this paper, we present a convex optimization problem to generate Center of Mass (CoM) and momentum trajectories of a walking robot, such that the motion robustly satisfies the friction cone constraints on uneven terrain. We adopt the Contact Wrench Cone (CWC) criterion to measure a robot's dynamical stability, which generalizes the venerable Zero Moment Point (ZMP) criterion. Unlike the ZMP criterion, which is ideal for walking on flat ground with unbounded tangential friction forces, the CWC criterion incorporates non-coplanar contacts with friction cone constraints. We measure the robustness of the motion using the margin in the Contact Wrench Cone at each time instance, which quantifies the capability of the robot to instantaneously resist external force/torque disturbance, without causing the foot to tip over or slide. For pre-specified footstep location and time, we formulate a convex optimization problem to search for robot linear and angular momenta that satisfy the CWC criterion. We aim to maximize the CWC margin to improve the robustness of the motion, and minimize the centroidal angular momentum (angular momentum about CoM) to make the motion natural. Instead of directly minimizing the non-convex centroidal angular momentum, we resort to minimizing a convex upper bound. We show that our CWC planner can generate motion similar to the result of the ZMP planner on flat ground with sufficient friction. Moreover, on an uneven terrain course with friction cone constraints, our CWC planner can still find feasible motion, while the outcome of the ZMP planner violates the friction limit.**

## I. Introduction

The first and foremost objective in humanoid control is to enable the robot to walk robustly without falling over. There has been a lot of progress in achieving this goal in recent years. For example, in the DARPA Robotics Challenge, the robot could traverse different types of terrain, including flat ground, tilted cinderblocks, and stairs [20], [11]. The planning approach in the aforementioned works relies on the venerable Zero Moment Point (ZMP) criterion[29], which asserts that if the center of pressure lies strictly within the foot support region, then the feet will not tip over [27]. Since its introduction almost half a century ago, the Zero Moment Point has gained great attention due to its simplicity. There has been a lot of research to plan the robot CoM trajectory, so as to satisfy the ZMP criterion [16], [10], [9], [28].

Although widely adopted, ZMP criterion has some severe limitations. First, it assumes that the feet are on flat ground. Second, it only guarantees that the feet will not tip over, by enforcing the normal contact force to point upward; it cannot restrain the feet from sliding, since the ZMP criterion ignores the friction cone constraint, and assumes that the tangential friction force can be infinite. Thus even if the ZMP lies strictly within the support region, the robot can still fall down due to foot sliding.

Fig. 1: Robot walking over uneven terrain course with friction cones (cyan)

In this paper we will adopt the Contact Wrench Cone (CWC) criterion, which requires that the total contact wrench lying within its admissible set, called the Contact Wrench Cone [15], [31]. In [15] it is proved that this criterion is equivalent to ZMP criterion when the feet are on flat ground with sufficient friction forces; moreover it can incorporate non-coplanar contact with friction cone constraints. There has been some work to plan a feasible motion using this criterion through non-convex optimization [7], [14]. In this paper, we aim to plan a robust motion with the CWC criterion through convex optimization.

The CWC notion can be used to determine not only the feasibility of a given motion, but also to measure its robustness. We adopt the robustness metric proposed by Barthelemy et al. [2], to quantify the capability of the robot to resist external force/torque (wrench) disturbance without breaking static contact. We call this metric the *Contact Wrench Cone margin*. Barthelemy et al. showed how to compute this robustness metric for a given motion; we will aim to explicitly optimize this metric by searching over the motion.

In [5], Caron et al. formulated a convex optimization problem to maximize the CWC margin, with given robot path (joint angles at each time sample), and search over the time intervals between each samples. In this paper, we will suppose that the footstep locations and timing are pre-specified, and we will search for the robot CoM and momentum trajectories through convex optimization.

Our key contribution in the paper is to formulate the CoM

*This work was supported by 6923036 Navy - ONR / Fy Appropriations Uncapped Funds

[1]Computer Science Artifitial Intelligence Lab, Massachusetts Institute of Technology daih,russt@csail.mit.edu

[2]Toyota Research Institute

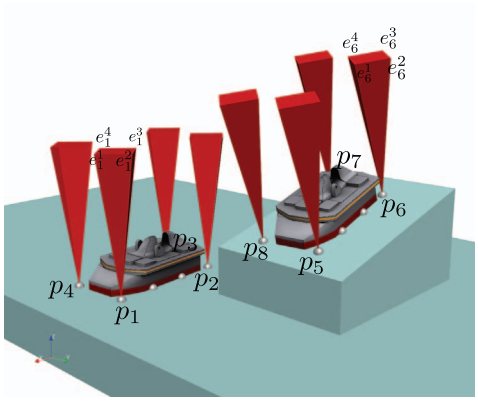


Fig. 2: The linearized friction cones at each corner of the feet.

and momentum generation problem as a *convex* optimization problem, rather than a non-convex problem, presented in the previous work [19], [14].

We will give a brief introduction on Contact Wrench Cone and its margin in Sec II. In Sec III we present the convex optimization problem to search for the robot CoM and momenta (linear and angular momentum). In Sec IV we will demonstrate the results for robot walking on flat ground (IV-A) and on a tilted terrain course with friction cone constraints (IV-B). We will conclude the paper in Sec.V.

## II. Background

The Contact Wrench Cone (CWC) can be used as a generalized stability criterion for robots making multiple contacts, subject to friction cone constraints [15], [31]. In this section, we will describe how to compute the CWC, how to enforce the stability criterion, and how to measure the robustness of the motion using this cone.

### A. Computing Contact Wrench Cone

The contact wrench cone (CWC) is the admissible set of the *total* contact wrench, which is computed by summing up the individual contact wrenches at each contact location. A wrench is the concatenation of a force and a torque. When we use linearized Coulomb friction cone model, we can compute the explicit form of the CWC. To illustrate how to obtain this explicit form, consider robot feet making multiple contacts, as shown in Fig. 2. At contact location $p_i$, the edges of the friction cone are $e_i^j, j = 1, \ldots, n_e$. Each edge is equivalent to a wrench (force/torque) $w_i^j$ expressed in the world coordinates

$$w_i^j = \begin{bmatrix} e_i^j \\ p_i \times e_i^j \end{bmatrix} \tag{1}$$

where $\times$ is the cross product between two 3-dimensional vectors.

According to the Coulomb friction model, when the contact point sticks to the ground, the contact force at each individual point $p_i$ is a non-negative combination of the edges $e_i^j$ of that friction cone. Thus for a robot making $n$ contacts at location $p_i, i = 1, \ldots, n$, the total contact wrench is the non-negative combination of the wrenches $w_i^j$ corresponding to every friction cone edge. As a result, the set of the total contact wrench is the convex cone of $w_i^j$

$$CWC = \text{ConvexCone}(w_i^j)\ i = 1, \ldots, n, j = 1, \ldots, n_e \tag{2}$$

where ConvexCone is the function to compute the convex cone combination, i.e., $\text{ConvexCone}(w_i^j \ldots, w_i^j) = \left\{ \sum_{i,j} \lambda_i^j w_i^j \mid \lambda_i^j \geq 0 \right\}$.

With pre-specified footstep locations generated by a footstep planner [8], [32], [21], the contact locations $p_i$ and the friction cone edges $e_i^j$ will both be given. Thus we can compute the Contact Wrench Cone as a conic polyhedron using (2), where $w_i^j$ are the candidate extreme rays of this conic polyhedron. This polyhedron can also be described by its facets, in the following form

$$CWC = \left\{ w | a_k^T w \leq 0, k = 1, \ldots, n_f \right\} \tag{3}$$

where $n_f$ is the number of facets in this polyhedron. $a_k \in \mathbb{R}^6$ is the normal vector of each facet. We can use the *double description method* [12] to convert this cone from the description with extreme rays (2) to the description with facets (3) [5]. Without loss of generality, we can assume that the normal vector $a_k$ of each facet has unit length. In the subsequent sections we will represent CWC as the intersection of halfspaces, as in (2). As we will see in subsections II-B and II-C, this representation empowers us to easily measure the stability and robustness of a motion using Contact Wrench Cone.

### B. Stability Criterion

We can use the Contact Wrench Cone to enforce a stability criterion for a walking robot [15], [31], that the total contact wrench has to lie within this cone. According to Newton's law, since the robot is only subject to contact forces and gravitational force, the total contact wrench should be equal to the rate of the robot momenta (linear and angular momentum) subtracting the gravitation wrench. As a result, the following inclusion condition should hold

$$\underbrace{\begin{bmatrix} m\ddot{r} \\ \dot{k}_O \end{bmatrix}}_{\text{rate of robot momenta}} - \underbrace{\begin{bmatrix} m\mathbf{g} \\ r \times m\mathbf{g} \end{bmatrix}}_{\text{gravitational wrench}} \in CWC \tag{4}$$

where $m$ is the robot mass, $r \in \mathbb{R}^3$ is the CoM of the robot, $k_O \in \mathbb{R}^3$ is the robot angular momentum about the origin of the world coordinate. $\mathbf{g} = [0\ 0\ -9.81]^T$ is the gravitational acceleration.

This Contact Wrench Cone criterion (4) is an extension of the Zero Moment Point (ZMP) criterion. When the feet are on flat ground with unbounded tangential friction force, the CWC criterion is equivalent to the ZMP criterion, as proved by Hirukawa et al. [15]. On the other hand, the CWC criterion holds when the contact locations are not co-planar. It also explicitly considers the friction cone constraints. As a result, it guarantees that the feet will not slide or tip over.

The CWC criterion is only a sufficient condition for a motion being dynamically feasible. It ignores the torque limits at each individual joints. Fortunately, many humanoids

are equipped with powerful actuators at all joints, so the joint torque limits are not violated in many cases. As a result, we can focus on the constraints on the 6 un-actuated degrees of freedom (DoF). The motion of these un-actuated DoFs is feasible if it satisfies the CWC criterion.

### C. Contact Wrench Cone Margin

The Contact Wrench Cone can be used to determine not only the feasibility of a motion, but also its robustness. To this end, we use the notion of Contact Wrench Cone margin, defined as follows [2], [5]

**Definition 1.** *Contact Wrench Cone margin is the smallest magnitude of the wrench disturbance being applied at a certain location, that the robot cannot resist, given the contact locations and friction cone constraints.*

A similar robustness metric has been used by the grasping community, to measure the quality of a force closure grasp [17], [6].

Algebraically, the Contact Wrench Cone margin is the maximum value of $\epsilon$, such that the contact wrench superimposed with the disturbance wrench is still within the Contact Wrench Cone, as long as the magnitude of the disturbance wrench is no larger than $\epsilon$. Namely

$$\mathcal{B}_\epsilon \subset CWC \tag{5}$$

$$\text{where } \mathcal{B}_\epsilon = \left\{ \underbrace{\begin{bmatrix} m\ddot{r} \\ \dot{k}_O \end{bmatrix} - \begin{bmatrix} m\mathbf{g} \\ r \times m\mathbf{g} \end{bmatrix}}_{\text{contact wrench}} + T(p_w)w \;\middle|\; w^T Q_w w \leq \epsilon^2 \right\}$$

where $Q_w \in \mathbb{R}^{6\times 6}$ is a symmetric matrix to encode the norm in the wrench space. $p_w$ is the pre-specified location where the disturbance wrench $w$ is applied. $T(p_w) \in \mathbb{R}^{6\times 6}$ is the transformation matrix that maps the wrench at $p_w$ to an equivalent wrench at the origin

$$T(p_w) = \begin{bmatrix} I_{3\times 3} & 0_{3\times 3} \\ \lfloor p_w \rfloor_\times & I_{3\times 3} \end{bmatrix} \tag{6}$$

where $\lfloor p_w \rfloor_\times \in \mathbb{R}^{3\times 3}$ is the skew symmetric matrix that represents the cross product with $p_w$. This skew-symmetric matrix has the following form for a vector $x \in \mathbb{R}^3$.

$$\lfloor x \rfloor_\times = \begin{bmatrix} 0 & -x_3 & x_2 \\ x_3 & 0 & -x_1 \\ -x_2 & x_1 & 0 \end{bmatrix} \tag{7}$$

Geometrically, the Contact Wrench Cone margin is the maximum radius of the ellipsoid $\mathcal{B}_\epsilon$ defined in (5), such that the ellipsoid is centered at the contact wrench, contained inside the Contact Wrench Cone.

Physically, the Contact Wrench Cone margin measures the capability of the robot to resist external wrench disturbance. We adopt it as the robustness metric for a walking motion. In this paper, we aim to explicitly optimize the robustness of the walking robot, by searching for the motion that maximizes the Contact Wrench Cone margin.

We can compute the Contact Wrench Cone margin $\epsilon$ analytically, as the smallest distance in the wrench space, from the contact wrench to each facet of the Contact Wrench Cone

$$\epsilon = \min_{k=1,\ldots,n_f} \bar{a}_k^T \begin{bmatrix} m\ddot{r} - m\mathbf{g} \\ \dot{k}_O - r \times m\mathbf{g} \end{bmatrix} \tag{8}$$

where $\bar{a}_k = -[a_k^T T(p_w) Q_w^{-1} T^T(p_w) a_k]^{-\frac{1}{2}} a_k$ is a given vector, as the contact location, the friction cone and the disturbance location are all pre-specified. The CWC margin can be equivalently formulated as the maximal value of the optimization problem

$$\max_{\epsilon} \quad \epsilon \tag{9}$$

$$\text{s.t } \epsilon \leq \bar{a}_k^T \begin{bmatrix} m\ddot{r} - m\mathbf{g} \\ \dot{k}_O - r \times m\mathbf{g} \end{bmatrix}, k = 1, \ldots, n_f \tag{10}$$

In Section III, we will use this formulation (10) to search for robot motion $r, \ddot{r}, \dot{k}_O$ in order to maximize the Contact Wrench Cone margin.

## III. Approach

In this section, we will present a convex optimization problem to generate robot CoM and angular momentum trajectories. We will show that we can maximize the Contact Wrench Cone margin to improve the robustness of the motion, and also to minimize the centroidal angular momentum (the angular momentum about the CoM) to make the motion more natural.

### A. Time discretization and integration

To formulate the motion planning problem as an optimization problem, we first discretize the motion by taking $N$ time samples. We search for the snapshots of the motion at each time knot through optimization, and then interpolate between the time samples to generate the trajectories. At the $i$th time sample, the variables we will optimize over include

- The CoM position $r[i]$ and its derivatives $\dot{r}[i], \ddot{r}[i]$.
- The angular momentum about the world origin $k_O[i]$ and its derivative $\dot{k}_O[i]$.
- The Contact Wrench Cone margin $\epsilon[i]$.

The square bracket $[i]$ indicates the time index. In the following sections, we will omit the time index when there is no ambiguity.

We suppose the timing of each knot is pre-specified by the footstep planner. We denote the given time interval between the $i$th and $i+1$th knot point as $dt[i]$. To interpolate the trajectory with snapshots at each time knot, we impose time integration constraints on the CoM, the angular momentum, and their derivatives. In this paper, for simplicity, we choose the backward Euler integration on CoM acceleration $\ddot{r}$, the mid-point interpolation for CoM velocity $\dot{r}$, and the backward Euler integration for the rate of angular momentum $\dot{k}_O$.

$$\forall i = 1, \ldots, N-1 \begin{cases} \dot{r}[i+1] - \dot{r}[i] = \ddot{r}[i+1]dt[i] \\ r[i+1] - r[i] = \frac{1}{2}(\dot{r}[i] + \dot{r}[i+1])dt[i] \\ k_O[i+1] - k_O[i] = \dot{k}_O[i+1]dt[i] \end{cases} \tag{11}$$

The time integration constraints above ((11)) are all linear constraints on the decision variables $r[i], \dot{r}[i], \ddot{r}[i], k_O[i], \dot{k}_O[i]$.

### B. Centroidal Angular Momentum

In order to generate natural walking motion, we need to regulate robot's angular momentum [25], [30], [14], [18]. We aim to track a desired centroidal angular momentum (momentum about the CoM). It is common to choose zero centroidal angular momentum as the reference trajectory. As some human experiments show that the centroidal angular momentum is kept small during walking [13]. In this paper, for simplicity we aim to minimize the centroidal angular momentum. Our approach is also applicable when the desired centroidal angular momentum is non-zero.

The centroidal angular momentum $k_G \in \mathbb{R}^3$ can be computed from robot angular momentum about the world origin $k_O$, and robot CoM $r$ and $\dot{r}$.

$$k_G = k_O - mr \times \dot{r} \tag{12}$$

We aim to minimize $|k_G|_1$, the $L_1$ norm of the centroidal angular momentum $k_G$. This norm can be formulated as the maximal value among linear functions of $k_G$

$$|k_G|_1 = \max_{i=1,\dots,8} \alpha_i^T k_G \tag{13}$$

where $\alpha_i \in \mathbb{R}^3, i = 1, \dots, 8, \alpha_i = [\pm 1, \pm 1, \pm 1]^T$.

Unfortunately, the centroidal angular momentum computed as in (12) is *not* a convex function of the decision variable $k_O, r, \dot{r}$. Specifically it involves the non-convex product between CoM position $r$ and its velocity $\dot{r}$. As a result, in order to plan the motion through convex optimization, we cannot minimize the $L_1$ norm of the centroidal angular momentum directly; instead, we will minimize a convex *upper bound* of the $L_1$ norm of $k_G$. We will show by minimizing this upper bound, we can effectively minimize $|k_G|_1$.

One such upper bound of $|k_G|_1$ can be obtained by considering the CoM bound. With pre-specified footstep locations, the admissible region of the CoM is also bounded, due to robot kinematics. We notice that the bounds on CoM $r$ will introduce an upper bound on $|k_G|_1$, by replacing $r$ in product $r \times \dot{r}$ with some appropriate value on the boundary of the CoM admissible region. To see this, we consider the two types of admissible regions, either a polytope (Fig. 3a) or an ellipsoid (Fig. 3b).

*1) Polytopic CoM region:* For a polytopic admissible region $\mathcal{P}_r$ with $n_r$ vertices $v_1, \dots, v_{n_r}$ (Fig. 3a), this polytope can also represented using its facets

$$\mathcal{P}_r : \{r | A_r r \le b_r\} \tag{14}$$

where each row of $A_r$ is the transpose of the normal vector on each facet of polytope $\mathcal{P}_r$. (14) are linear constraints on CoM position $r$.

When the admissible region for the CoM is a polytope $\mathcal{P}_r$ as in Fig. 3a, an upper bound of $|k_G|_1$ can be obtained by replacing the CoM $r$ with one vertex of the polytope. To see

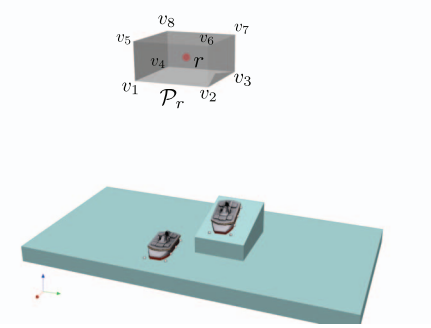


(a) Polytopic CoM region

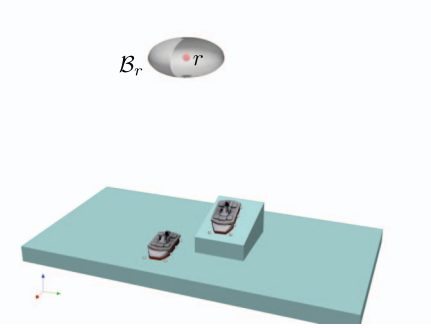


(b) Ellipsoidal CoM region

Fig. 3: Footstep locations and the admissible region for CoM.

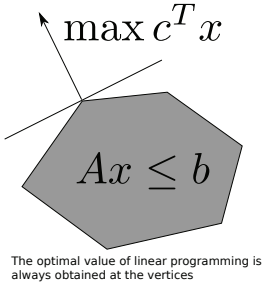


Fig. 4: Linear programming

this, we formulate the following optimization problem $\mathbb{P}_1$ to minimize the $L_1$ norm of centroidal angular momentum, with optimal value $p_1^*$.

$$\mathbb{P}_1 : p_1^* = \min_{\substack{\dot{r}, k_O \\ r \in \mathcal{P}_r}} \max_{i=1,\dots,8} \alpha_i^T (k_O - mr \times \dot{r}) \tag{15}$$

An upper bound of $p_1^*$ is obtained if we maximize over CoM position $r$ first, and then minimize over the rest of the variables. This new optimization problem $\mathbb{P}_2$ has optimal value $p_2^*$.

$$\mathbb{P}_2 : p_2^* = \min_{\dot{r}, k_O} \max_{r \in \mathcal{P}_r} \max_{i=1,\dots,8} \alpha_i^T (k_O - mr \times \dot{r}) \tag{16}$$

$p_2^* \ge p_1^*$ since (16) maximizes over CoM position $r$, where (15) minimizes over it.

An important observation is that we can explicitly compute the maximization over $r$ within polytope $\mathcal{P}_r$. From linear programming, we know that the maximization of a linear function within a polytope is always obtained at one vertex of the polytope, as shown in Fig. 4. We can thus replace the CoM $r$ with each vertex of the polytope, and take the maximal value among all these substitutions as an upper

bound of $|k_G|_1$. Namely, we transform $p_2^*$ in (16) as

$$\mathbb{P}_2 : p_2^* = \min_{\dot{r},k_O} \max_{\substack{i=1,\dots,8 \\ r\in\mathcal{P}_r}} \alpha_i^T(k_O - mr\times\dot{r}) \tag{17a}$$

$$= \min_{\dot{r},k_O} \max_{\substack{i=1,\dots,8 \\ j=1,\dots,n_r}} \alpha_i^T(k_O - mv_j\times\dot{r}) \tag{17b}$$

where $v_j, j = 1,\dots,n_r$ are the vertices of the polytope $\mathcal{P}_r$.

To write the upper bound of $|k_G|_1$ in (17b) as a convex constraint, we introduce a slack variable $s$ to represent the upper bound, with the following linear constraints

$$s \geq \alpha_i(k_O - mv_j\times\dot{r})\ \forall i = 1,\dots,8, j = 1,\dots,n_r \tag{18}$$

(18) are linear, and thus convex. We can minimize $s$, the upper bound of centroidal angular momentum, with these linear constraints.

*2) Ellipsoidal CoM region:* If the ellipsoidal admissible region (Fig. 3b) is used, we formulate this ellipsoid $\mathcal{B}_r$ as

$$\mathcal{B}_r = \{r|(r-r^*)^T Q_r (r-r^*) \leq 1\} \tag{19}$$

where $r^*$ is the center of the ellipsoid. (19) is a convex quadratic constraint on CoM position $r$. It can also be formulated as a *second-order cone* constraint [1].

Similar to the polytope case, we can obtain an upper bound of the $L_1$ norm of the centroidal angular momentum, with this ellipsoidal admissible region. We define minimizing $|k_G|_1$ as the optimal value $p_1^*$ of the following optimization problem.

$$\mathbb{P}_1 : p_1^* = \min_{\substack{\dot{r},k_O \\ r\in\mathcal{B}_r}} \max_{i=1,\dots,8} \alpha_i^T(k_O - mr\times\dot{r}) \tag{20}$$

We define a new optimization problem $\mathbb{P}_2$ to first maximize over the CoM within the ellipsoid

$$\mathbb{P}_2 : p_2^* = \min_{\dot{r},k_O} \max_{\substack{i=1,\dots,8 \\ r\in\mathcal{B}_r}} \alpha_i^T(k_O - mr\times\dot{r}) \tag{21a}$$

$$= \min_{\dot{r},k_O} \max_{i=1,\dots,8} \left(\alpha_i^T k_O + \max_{r\in\mathcal{B}_r} m\alpha_i^T(\dot{r}\times r)\right) \tag{21b}$$

$$= \min_{\dot{r},k_O} \max_{i=1,\dots,8} \Bigg(\alpha_i^T k_O + m\alpha_i^T(\dot{r}\times r^*) + m\sqrt{\dot{r}^T \lfloor\alpha_i\rfloor_\times^T Q_r^{-1} \lfloor\alpha_i\rfloor_\times \dot{r}}\Bigg) \tag{21c}$$

where $\lfloor\alpha_i\rfloor_\times \in \mathbb{R}^{3\times3}$ is the skew-symmetric matrix representing the cross product with $\alpha_i$, as defined in (7).

The equality from (21b) to (21c) holds because the maximization of a linear function over an ellipsoid can be computed explicitly. A simple example is $\max_{x^Tx\leq1} c^Tx = \sqrt{c^Tc}$.

To write the upper bound $p_2^*$ in (21c) as a convex constraint, we introduce a slack variable $s$ to represent the upper bound, with the following constraints

$$s - \alpha_i^T k_O - m\alpha_i^T(\dot{r}\times r^*) \geq m\sqrt{\dot{r}^T \lfloor\alpha_i\rfloor_\times^T Q_r^{-1} \lfloor\alpha_i\rfloor_\times \dot{r}}\quad \forall i = 1,\dots,8 \tag{22}$$

The left-hand side of (22) is a linear function of decision variables $s, k_O, \dot{r}$, the right-hand side of (22) is a weighted 2-norm of variable $\dot{r}$, thus (22) is a *second-order cone* constraint, which is a special convex constraint.

The relaxation of the original non-convex function $\mathbb{P}_1$ to the convex upper bound in $\mathbb{P}_2$ can also be interpreted through *robust optimization* [3]. We can regard CoM position $r$ as the uncertain parameter of the optimization problem $\mathbb{P}_1$, and we want to minimize the worst-case value of $\mathbb{P}_1$ under parameter uncertainty. This worst-case value is an upper bound of $p_1^*$, and we can compute the upper bound through a convex optimization. For more details on robust optimization, the readers can refer to [3], [4].

To summarize III-B, we aim to minimize the centroidal angular momentum in order to obtain a natural walking motion. To this end, we minimize a convex upper bound of the $L_1$ norm of centroidal angular momentum $|k_G|_1$, by leveraging the admissible region on CoM position. When the admissible region is a polytope, we can minimize $|k_G|_1$ through linear programming; when the region is an ellipsoid, we can minimize $|k_G|_1$ through second-order conic programming.

### C. Objective function

We propose three parallel goals for the optimization problem

1) Maximizing the Contact Wrench Cone margin $\epsilon$ to make the motion robust.
2) Minimizing the upper bound of $L_1$ norm of centroidal angular momentum $s$ to make the motion natural.
3) Minimizing the CoM acceleration $\ddot{r}$ to make the motion smooth.

Thus we formulate the objective function as a weighted sum of $\epsilon, s$ and $\ddot{r}$

$$\min_{\substack{r,\dot{r},\ddot{r}, \\ k_O,\dot{k}_O, \\ \epsilon,s}} \sum_{i=1}^{N} -c_\epsilon\epsilon[i] + c_s s[i] + c_{\ddot{r}}\ddot{r}[i]^T\ddot{r}[i] \tag{23}$$

where $c_\epsilon, c_s, c_{\ddot{r}}$ are all positive constants.

The constraints for the optimization problems include the time integration constraints (11), the CWC margin constraint (10), the CoM bound constraints (14) or (19), the centroidal angular momentum upper bound constraint (18) or (22). The problems end up being Quadratic Programming if we approximate the CoM admissible region with a polytope, or a second-order conic programming if we approximate it with an ellipsoid.

## IV. Results

In this section, we will show that our Contact Wrench Cone (CWC) planner can generate a robust walking motion with CoM and angular momentum trajectories. We tested two types of terrain using an Atlas robot model [23]. Our result is very similar to that of a Zero Moment Point (ZMP) planner when the robot walks on flat ground, since the Contact Wrench Cone criterion is equivalent to the Zero

Moment Point criterion on flat ground with sufficient friction. We also show that when planning walking motion on an uneven terrain course with friction cone constraints, our CWC planner can generate feasible motion, while the result of the ZMP planner violates the friction cone constraints.

### A. Walking on flat ground

For a robot walking on flat ground with friction coefficient equals to 1, we compare the results of the CWC planner to that of the ZMP planner [28]. We use either a polytopic admissible region or an ellipsoidal admissible region for the CoM. The ZMP planner attempts to minimize the distance from the ZMP to the center of the support region on the ground. At each time sample, we set the disturbance point $p_w$ is the center of the feet region. The admissible region is centered at 0.8m above the middle of the feet region; it is either a box of size $0.3m \times 0.3m \times 0.1m$, or an ellipsoid with axes length $0.3m \times 0.3m \times 0.1m$.

We first compare the CoM trajectories on the flat ground, shown in Fig. 5. The result of the CWC planner is close to that of the ZMP planner. We point out here that unlike the Linear Inverted Pendulum model used for the ZMP planner, which requires the CoM height being a constant; for the CWC planner, we do not have that constraint, and the CoM height changes in Fig. 5. When using polytopic CoM region, the CoM height descents in Fig. 5a occur during the single support phase of the robot.

We draw the centroidal angular momentum coming out of the CWC planners, together with its upper bound in Fig. 6. The magnitude of the centroidal angular momentum is small. It is in the same scale as the human experiment data, reported in [13]

We also draw the Contact Wrench Cone margin of both CWC and ZMP planner results in Fig. 7. The peaks correspond to the double support phase; when there are more contact points, the Contact Wrench Cone is enlarged, thus the margin is increased.

The trajectory comprises of 549 time samples, and the optimization problem has 9333 decision variables. We use an Intel i7 machine with Mosek 8 beta[22]. The solver time is 3.5 seconds for a polytopic admissible CoM region, and 1.8 seconds for an ellipsoidal admissible CoM region.

We show the scalability of the computation time in Fig.8. The computation time scales almost linearly w.r.t the number of time samples.

### B. Tilted terrain course

We also test the planners on uneven terrain with friction cone constraints. We modify the terrain course from the DARPA Robotics Challenge [26], with friction coefficient being 0.4. This terrain course is visualized in Fig. 9. With the pre-specified foot locations from a footstep planner [8], we first obtain a CoM trajectory from the ZMP planner [28]. When we examine the ZMP trajectory by computing the corresponding contact force, we observe that at some time samples, the ground reaction force falls outside of the friction cone, as shown in Fig. 10a . Thus the robot foot would

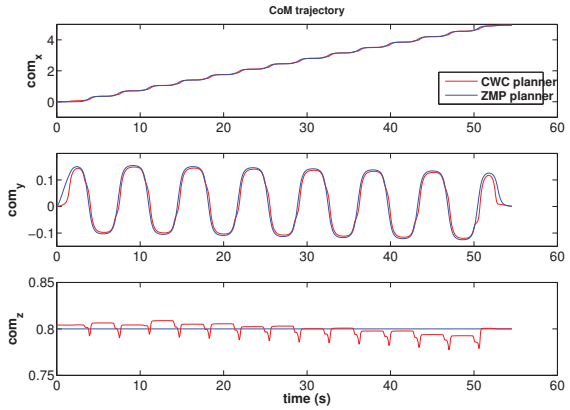


(a) Polytopic CoM admissible region

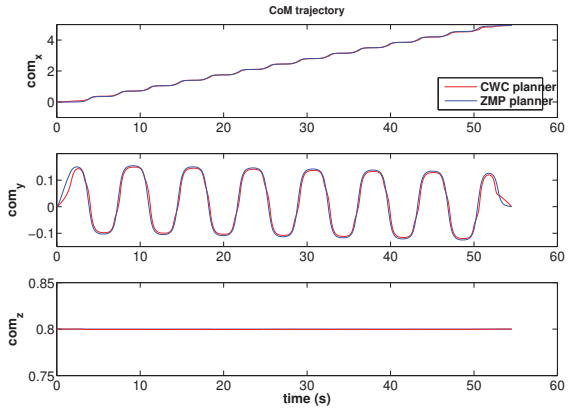


(b) Ellipsoidal CoM admissible region

Fig. 5: CoM trajectories in three axes

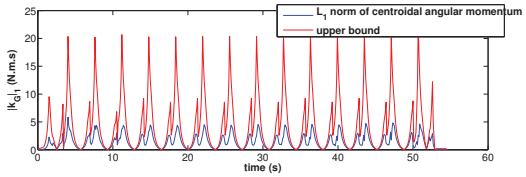


(a) Polytopic CoM admissible region

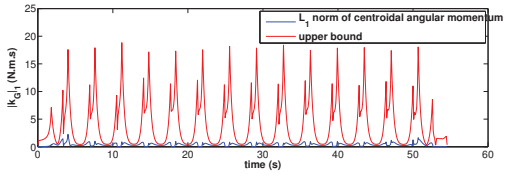


(b) Ellipsoidal CoM admissible region

Fig. 6: $L_1$ norm of centroidal angular momentum, and its upper bound on flat ground

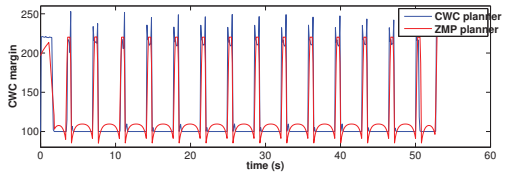


(a) Polytopic CoM admissible region

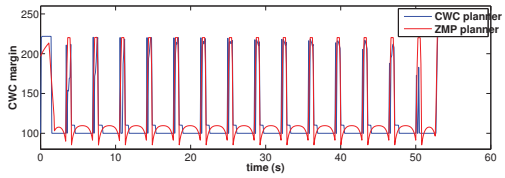


(b) Ellipsoidal CoM admissible region

Fig. 7: Contact Wrench Cone margin on flat ground

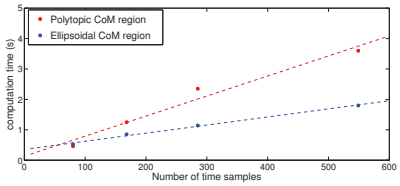


Fig. 8: Scalability of computation time

slide when executing this plan, resulting in the robot falling over. This problem is caused by ZMP planner's ignorance of friction cone on uneven ground.

As a comparison, we run our CWC planners on the same terrain course. The CoM trajectories are visualized in Fig. 9. These trajectories from the CWC planners are quite different from the ZMP planner's result. We also examine the contact force at the same moment when that from the ZMP planner violates the friction cone constraint, visualized in Fig. 10b,10c; the friction force from the CWC planner stays within the friction cone.

We draw the centroidal angular momentum from the CWC planner, together with its upper bound in Fig. 11. The centroidal angular momentum is kept small, and it's in the same scale as the flat ground walking case in Fig. 6.

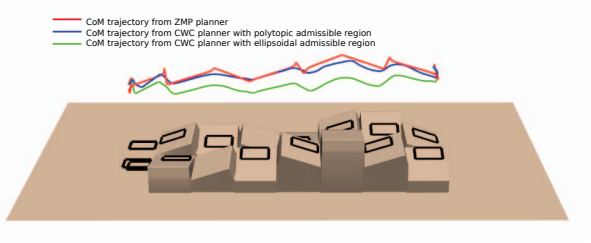


Fig. 9: Tilted terrain, the pre-specified footsteps (black rectangles) and CoM trajectories

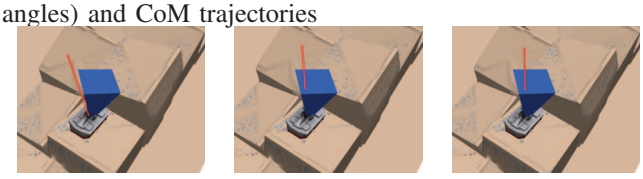

(a) ZMP planner (b) CWC planner, polytopic CoM region (c) CWC planner, ellipsoidal CoM region

Fig. 10: Contact force (red) and the friction cone (blue).

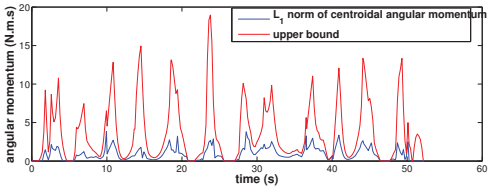


(a) Polytopic admissible CoM region

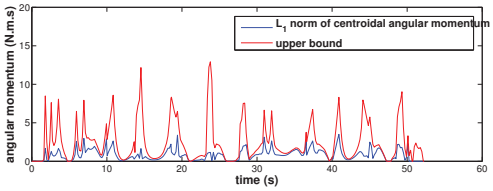


(b) Ellipsoidal admissible CoM region

Fig. 11: Centroidal angular momentum and its upper bound

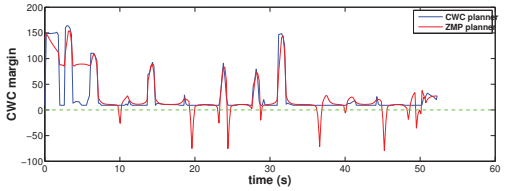


(a) Polytopic admissible CoM region

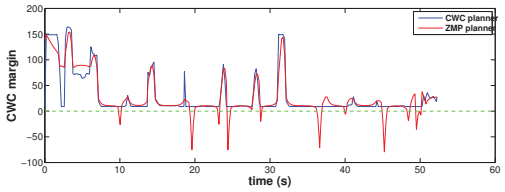


(b) Ellipsoidal admissible CoM region

Finally, we draw the CWC margin from each planner result. As we mentioned before, the result of the ZMP planner violates the friction cone constraints. This agrees with the CWC margin being negative for some time samples in the ZMP planner result. On the contrary, the margins stay uniformly positive for the results of the CWC planner. Thus the CWC planner can successfully plan feasible motion satisfying the friction cone constraints on uneven terrain, while the ZMP planner can fail.

The trajectory comprises of 268 time samples. The optimization problem has 4556 decision variables. The solver time is 7.5s for polytopic CoM admissible region with Gurobi solver [24], and 2.1s for ellipsoidal CoM admissible region with Mosek 8 beta [22].

## V. Conclusion and Discussion

In this paper, we present a planner to optimize the robot CoM motion and angular momentum. We formulate a convex optimization problem to maximize the Contact Wrench Cone (CWC) margin, which measures the robustness of the motion. We also minimize the centroidal angular momentum to make the motion more robust. Since the centroidal angular momentum is a non-convex function, we resort to minimizing a convex upper bound. We show that our Contact Wrench Cone planner generates results similar

to that of the Zero Moment Point planner on flat ground with sufficient friction. On a tilted terrain course with friction cone constraints, our CWC planner successfully generates a feasible motion, while the result of the ZMP planner violates the friction cone constraints.

One candidate extension of this paper is to consider a tighter upper bound of the $L_1$ norm of the centroidal angular momentum. In sub-section III-B we obtain an upper bound by considering the bounds on the CoM position. We can alternatively obtain another upper bound by considering the bounds on the CoM velocity. A tighter upper bound is the minimal value between these two upper bounds. We can minimize this minimal value between two upper bounds using mixed-integer convex optimization.

Another candidate extension is to include hand contact with the environment, as Caron et al. did in [5]. We did not use hand contact in this work, as it is tricky to model the contact force constraint for hand contact, as the hand contact region might not be a flat surface as the feet.

## VI. Acknowledgement

This work is supported by 6923036 Navy - ONR / Fy Appropriations Uncapped Funds.

## References

[1] Farid Alizadeh and Donald Goldfarb. Second-order cone programming. *Mathematical programming*, 95(1):3–51, 2003.

[2] Sebastien Barthelemy and Philippe Bidaud. Stability measure of postural dynamic equilibrium based on residual radius. In *Advances in Robot Kinematics: Analysis and Design*, pages 399–407. Springer, 2008.

[3] Aharon Ben-Tal and Arkadi Nemirovski. Robust convex optimization. *Mathematics of operations research*, 23(4):769–805, 1998.

[4] Dimitris Bertsimas, David B Brown, and Constantine Caramanis. Theory and applications of robust optimization. *SIAM review*, 53(3):464–501, 2011.

[5] Stephane Caron, Quang-Cuong Pham, and Yoshihiko Nakamura. Leveraging cone double description for multi-contact stability of humanoids with applications to statics and dynamics. *Robotics: Science and System*, 2015.

[6] Hongkai Dai, Anirudha Majumdar, and Russ Tedrake. Synthesis and optimization of force closure grasps via sequential semidefinite programming. In *International Symposium on Robotics Research*, 2015.

[7] Hongkai Dai, Andrés Valenzuela, and Russ Tedrake. Whole-body motion planning with centroidal dynamics and full kinematics. *IEEE-RAS International Conference on Humanoid Robots*, 2014.

[8] Robin Deits and Russ Tedrake. Footstep planning on uneven terrain with mixed-integer convex optimization. In *Proceedings of the 2014 IEEE/RAS International Conference on Humanoid Robots (Humanoids 2014)*, Madrid, Spain, 2014.

[9] Dimitar Dimitrov, Alexander Sherikov, and Pierre-Brice Wieber. A sparse model predictive control formulation for walking motion generation. In *Proceedings of the 2011 IEEE/RSJ International Conference on Intelligent Robots and Systems*, 2011.

[10] Dimitar Dimitrov, Pierre-Brice Wieber, Hans Joachim Ferreau, and Moritz Diehl. On the implementation of model predictive control for on-line walking pattern generation. In *Robotics and Automation, 2008. ICRA 2008. IEEE International Conference on*, pages 2685–2690. IEEE, 2008.

[11] Siyuan Feng, Eric Whitman, X Xinjilefu, and Christopher G Atkeson. Optimization-based full body control for the darpa robotics challenge. *Journal of Field Robotics*, 32(2):293–312, 2015.

[12] Komei Fukuda and Alain Prodon. Double description method revisited. In *Combinatorics and computer science*, pages 91–111. Springer, 1996.

[13] Hugh Herr and Marko Popovic. Angular momentum in human walking. *Journal of Experimental Biology*, 211(4):467–481, 2008.

[14] Alexander Herzog, Nicholas Rotella, Stefan Schaal, and Ludovic Righetti. Trajectory generation for multi-contact momentum control. In *Humanoid Robots (Humanoids), 2015 IEEE-RAS 15th International Conference on*, pages 874–880. IEEE, 2015.

[15] H Hirukawa, S Hattori, K Harada, S Kajita, K Kaneko, F Kanehiro, K Fujiwara, and M Morisawa. A universal stability criterion of the foot contact of legged robots - Adios ZMP. *Proc. of the IEEE Int. Conf. on Robotics and Automation*, pages 1976–1983, May 2006.

[16] S. Kajita, F. Kanehiro, K. Kaneko, K. Fujiware, K. Harada, K. Yokoi, and H. Hirukawa. Biped walking pattern generation by using preview control of zero-moment point. In *ICRA IEEE International Conference on Robotics and Automation*, pages 1620–1626. IEEE, Sep 2003.

[17] David Kirkpatrick, Bhubaneswar Mishra, and Chee-Keng Yap. Quantitative steinitz's theorems with applications to multifingered grasping. *Discrete & Computational Geometry*, 7(1):295–318, 1992.

[18] Koolen, Twan, Bertrand, Sylvain, Thomas, Gray, De Boer, Tomas, Wu, Tingfan, Smith, Jesper, Englsberger, Johannes, Pratt, and Jerry. Design of a momentum-based control framework and application to the humanoid robot atlas. Aug 2015.

[19] M Kudruss, Maximilien Naveau, Olivier Stasse, Nicolas Mansard, C Kirches, Philippe Soueres, and K Mombaur. Optimal control for whole-body motion generation using center-of-mass dynamics for predefined multi-contact configurations. In *Humanoid Robots (Humanoids), 2015 IEEE-RAS 15th International Conference on*, pages 684–689. IEEE, 2015.

[20] Scott Kuindersma, Robin Deits, Maurice Fallon, Andrés Valenzuela, Hongkai Dai, Frank Permenter, Twan Koolen, Pat Marion, and Russ Tedrake. Optimization-based locomotion planning, estimation, and control design for the Atlas humanoid robot. *Autonomous Robots*, 40(3):429–455, 2016.

[21] Philipp Michel, Joel Chestnutt, James Kuffner, and Takeo Kanade. Vision-guided humanoid footstep planning for dynamic environments. In *Humanoid Robots, 2005 5th IEEE-RAS International Conference on*, pages 13–18. IEEE, 2005.

[22] APS Mosek. The mosek optimization software. *Online at http://www.mosek.com*, 54, 2010.

[23] Gabe Nelson, Aaron Saunders, Neil Neville, Ben Swilling, Joe Bondaryk, Devin Billings, Chris Lee, Robert Playter, and Marc Raibert. Petman: A humanoid robot for testing chemical protective clothing. *Journal of the Robotics Society of Japan*, 30(4):372–377, 2012.

[24] Gurobi Optimization et al. Gurobi optimizer reference manual. *URL: http://www. gurobi. com*, 2012.

[25] David E. Orin, Ambarish Goswami, and Sung-Hee Lee. Centroidal dynamics of a humanoid robot. *Autonomous Robots*, (September 2012):1–16, jun 2013.

[26] Gill Pratt and Justin Manzo. The darpa robotics challenge [competitions]. *IEEE Robotics & Automation Magazine*, 20(2):10–12, 2013.

[27] Philippe Sardain and Guy Bessonnet. Forces acting on a biped robot. Center of Pressure – Zero Moment Point. *IEEE Trans. on Systems, Man, and Cybernetics - Part A: Systems and Humans*, 34(5):630–637, Sep 2004.

[28] Russ Tedrake, Scott Kuindersma, Robin Deits, and Kanako Miura. A closed-form solution for real-time ZMP gait generation and feedback stabilization. In *Proceedings of the International Conference on Humanoid Robotics*, Seoul, Korea, November 2015.

[29] Miomir Vukobratovic and Davor Juricic. Contribution to the synthesis of biped gait. *Biomedical Engineering, IEEE Transactions on*, (1):1–6, 1969.

[30] Patrick M Wensing and David E Orin. Improved computation of the humanoid centroidal dynamics and application for whole-body control. *International Journal of Humanoid Robotics*, page 1550039, 2015.

[31] Pierre-Brice Wieber. On the stability of walking systems. In *Proceedings of the International Workshop on Humanoid and Human Friendly Robots*, 2002.

[32] Ye Zhao and Luis Sentis. A three dimensional foot placement planner for locomotion in very rough terrains. In *Humanoid Robots (Humanoids), 2012 12th IEEE-RAS International Conference on*, pages 726–733. IEEE, 2012.